

Constructing mock catalogues for the REFLEX II galaxy cluster sample

A. Balaguera-Antolínez^{1,2*}, Ariel G. Sánchez², H. Böhringer², C. Collins³

¹*Argelander Institute für Astronomie, Auf dem Hügel 71, D-53121 Bonn, Germany*

²*Max Planck Institute für Extraterrestrische Physik, D-85748, Garching, Germany*

³*Astrophysics Research Institute, Liverpool John Moores University, Birkenhead, Wirral CH41 1LD, U.K.*

4 November 2018

ABSTRACT

We describe the construction of a suite of galaxy cluster mock catalogues from N-body simulations, based on the properties of the new ROSAT-ESO Flux-Limited X-Ray (REFLEX II) galaxy cluster catalogue. Our procedure is based on the measurements of the cluster abundance, and involves the calibration of the underlying scaling relation linking the mass of dark matter haloes to the cluster X-ray luminosity determined in the *ROSAT* energy band 0.1 – 2.4 keV. In order to reproduce the observed abundance in the luminosity range probed by the REFLEX II X-ray luminosity function ($0.01 < L_X / (10^{44} \text{erg s}^{-1} h^{-2}) < 10$), a mass-X ray luminosity relation deviating from a simple power law is required. We discuss the dependence of the calibration of this scaling relation on the X-ray luminosity and the definition of halo masses and analyse the one- and two-point statistical properties of the mock catalogues. Our set of mock catalogues provides samples with self-calibrated scaling relations of galaxy clusters together with inherent properties of flux-limited surveys. This makes them a useful tool to explore different systematic effects and statistical methods involved in constraining both astrophysical and cosmological information from present and future galaxy cluster surveys.

Key words: cosmology: – large-scale structure of Universe - X-rays: galaxies - clusters

1 INTRODUCTION

Mock catalogues have become a key tool to assess the statistical methods employed in the analysis of redshift galaxy surveys, mainly concerning the study of the large-scale structure of the Universe (e.g Cole et al. 2005; Cabre et al. 2009; Sánchez et al. 2009; Percival et al. 2010; Norberg et al. 2011). Such tools have been usually constructed following two methods, the first being based on log-normal realizations of the matter density field (Coles & Jones 1991), and the second based on the use of N-body simulations. The log-normal catalogues can be produced in a shorter time period, and can be designed such that the final suite of mock observations share the same clustering properties as that of real data (e.g Percival et al. 2004; Cole et al. 2005). On the other hand, N-body simulations have the advantage of properly characterising the dynamical evolution and the growth of structures in the non-linear regime, providing a tool to test theoretical predictions for the abundance of dark matter

haloes (e.g Warren et al. 2006; Tinker 2008; Crocce et al. 2009) as well as on the non-linear evolution of gravitational clustering of matter, dark matter haloes and galaxies (e.g Evrard et al. 2002; Springel et al. 2005; Angulo et al. 2008; McBride et al. 2009; Cai et al. 2009; Teyssier et al. 2009). In the context of galaxy clusters surveys, the combination of cosmological N-body simulations, a precise understanding of the survey selection function and a set of cluster-mass proxies is required for the construction of mock catalogues containing the relevant structural and dynamical properties of these objects, such as their masses, X-ray luminosities, spectral temperatures, fluxes and peculiar velocities, among others. This provides a control sample to analyse the possible systematic effects in the determination of scaling relations and/or cosmological parameters, together with the possibility to assess the capability of future galaxy cluster surveys (e.g *eROSITA*¹) to push the constraints on the latter to higher precision (e.g Vikhlinin et al. (2009); Pillepich et al. (2011)).

* E-mail: abalan@astro-uni.bonn.de

¹ <http://www.mpe.mpg.de/erossita/>

In the context of cosmology probed by the clustering of galaxy clusters, previous analyses (e.g. Retzlaff et al. 1998; Schuecker et al. 2001) used cosmological N-body simulations in order to determine statistical properties such as covariance matrices associated to different measurements of abundance and clustering. On smaller scales, hydro-N-body simulations are widely used to explore the influence of non-thermal processes such as AGN and Supernova feedback on the cluster scaling relations (e.g. Evrard et al. 2002; Borgani et al. 2005; Stanek et al. 2010; Short et al. 2010). The implementation of the baryonic physics required to model these astrophysical processes in large cosmological simulations is challenging and it would demand extremely large computational resources. This leads to the necessity to implement semi-analytic models, which in the case of galaxy clusters refers to the cluster scaling relations, such that the mock catalogues match the observed properties of these objects.

This is the second of a series of papers dedicated to the analysis of the new REFLEX II galaxy cluster catalogue. A first paper (Balaguera-Antolínez et al. (2011), hereafter Paper I) was focused on the clustering analysis of this new sample through the power spectrum. In that work, a set of mock catalogues was used to determine the covariance matrix of the cluster power spectrum and thereby assess the statistical methods implemented in that analysis. In this paper we describe the construction of that suite of mock catalogues, which have been designed to reproduce basic properties of the REFLEX II sample (e.g. survey geometry, selection function, cluster abundance, etc.). A key ingredient in the construction of realistic cluster mock catalogues using N-body simulations is the assignment of luminosities to the dark matter haloes.

Owing to the fact that the one-point statistics (e.g. abundance) of galaxy clusters (as well as their clustering) are sensitive to the underlying mass M -X ray luminosity L_X relation (hereafter M - L_X) (e.g. Voit 2005), it is important to have a scaling relation consistent with both the observed cluster abundance and a halo mass-function in N-body simulations. Accordingly, instead of assigning luminosities using scaling relations found in the literature (see for instance the scaling relations obtained by Reiprich & Böhringer (1999); Stanek et al. (2006); Maughan (2007); Pratt et al. (2009); Mantz et al. (2010)), we calibrate the M - L_X based on the X-ray luminosity function (XLF hereafter) of the REFLEX II sample. We discuss the main features of the scaling relation, though it is not the scope of this paper to develop a deep analysis on this topic.

We also briefly describe the two-point statistics of our mock catalogues (broadly described in Fourier space in Paper I) and show how these can be used to determine covariance matrices in order to develop constraints on cosmological parameters based on likelihood analysis (Sánchez et al., in preparation). The worth of our set of mock catalogues is reflected in their physical and observational content. These are translated to the covariance matrix of the cluster power spectrum (or correlation function) and its capability to properly account for non-linear evolution of the matter density field, dependencies of clustering strength with the underlying scaling relations and systematics effects introduced by the survey selection function. In that sense, the set of REFLEX II mock catalogues introduced

in this paper represents an improvement in the analysis of this sample, compared to previous works (e.g. Collins et al. 2000; Schuecker et al. 2001) based on the REFLEX sample (Böhringer et al. 2001).

The outline of this paper is as follows. In § 2 we briefly introduce the REFLEX II galaxy cluster catalogue and in § 2.2 we describe the measurement and parameterisation of the REFLEX II XLF. In § 3 we introduce the N-body simulations and discuss the procedure we follow to calibrate the underlying M - L_X relation (§ 3.2 and § 3.3). In § 4 we discuss some of the most relevant properties of the mock catalogues. Finally, we end with our main conclusions in § 5.

We adopt a fiducial cosmological model based on a flat Λ CDM Universe with a matter energy density parameter of $\Omega_{\text{mat}} = 0.25$, a dimensionless Hubble parameter $h = 0.7$ (in units of $100 \text{ km s}^{-1} \text{ Mpc}^{-1}$) and a rms of mass fluctuations of $\sigma_8 = 0.773$. Unless otherwise stated, redshifts, distances, fluxes, luminosities, power spectra and mass functions are calculated with this set of cosmological parameters. Throughout this paper we always refer to the rest-frame X-ray luminosity in the *ROSAT* energy band $0.1 - 2.4 \text{ keV}$ determined under the assumption of spherical overdensities (SO hereafter) characterised by $\Delta = 500$ (i.e. the mean matter density of the cluster is 500 times the critical density of the Universe). We will frequently refer to *a set of realizations*, namely, the N-body simulations of dark matter haloes. We warn the reader not to confuse these with the *mock catalogues*, which refers to the set of REFLEX II-like catalogues.

2 THE REFLEX II CATALOGUE

2.1 The REFLEX II sample

The REFLEX catalogue is based on the ROSAT All-Sky Survey (RASS, Truemper 1993), where galaxy cluster candidates are detected as X-ray sources coinciding with galaxy concentrations in optical sky survey images (Böhringer et al., in preparation). The final identifications and redshift measurements come from complementary follow-up observations as described by Guzzo et al. (2009), yielding spectroscopic redshifts for 860 clusters with flux limit of $1.8 \times 10^{-12} \text{ erg s}^{-1} \text{ cm}^{-2}$ in the *ROSAT* energy band and approximately 6 per-cent incompleteness in redshift follow-up. The missing redshifts are currently being obtained through observations at La Silla. While a detailed description of the construction of the catalogue and the selection function will be given in forthcoming papers (Böhringer et al. in prep.), Paper I presents a brief summary of the main steps followed in the derivation of the cluster parameters and the characterisation of the survey selection function. Here we briefly summarize the aspects that are more relevant to the construction of the mock catalogues.

In our analysis we used the X-ray luminosities corrected for missing flux in the *ROSAT* energy band. The error in the measurement of the flux varies through the REFLEX II sample, depending on parameters such as the observed flux and the exposure time associated with each cluster. In order to keep the analysis simple, for the construction of the mock catalogues we adopted a normal distribution with a width

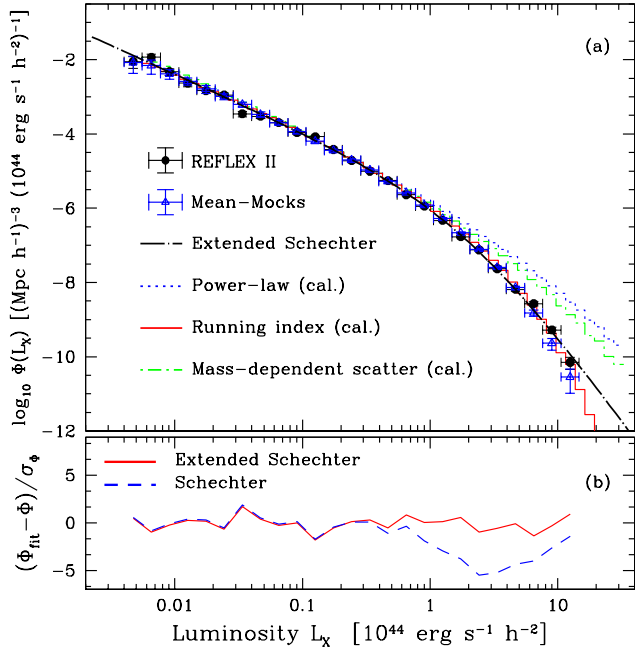


Figure 1. (a) The filled points with error bars correspond to the measurement of the REFLEX II X-ray luminosity function $\Phi(L_X)$. The black dot-dashed line represents the best fitting extended-Schechter function, defined in Eq. (1), to this measurement. The red solid, blue-dotted and green dot-dashed histograms represent the mean luminosity distribution determined from the ensemble of 50 realizations of the L-BASICC II simulation using haloes with X-ray luminosities assigned according to i) a $M-L_X$ relation given by Eq. (4) (running index) with the set (a, b, c) calibrated according to § 3.2, ii) a power-law $M-L_X$ relation and iii) a power-law with mass-dependent scatter (§ 3.4), respectively. The triangles represent the mean luminosity function from the final set of 100 mock catalogues. Panel (b) shows the difference between the measurements and the Schechter and extended Schechter fits in units of the standard deviation.

$\sigma_{L_X} = 0.2L_X$ (20 per cent error in the X-ray luminosity), which fairly characterizes the flux errors in the REFLEX II sample.

The REFLEX II sensitivity map can be described by dividing the surveyed area (13924 deg² in the southern hemisphere) into $N_{\text{pix}} = 13952$ pixels of approximately equal area of 1 deg². Depending on its exposure time, the limiting luminosity $L_X^{\text{lim}}(z)$ for each pixel was tabulated in the range $0 \leq z \leq 0.8$ assuming a nominal flux limit. This defines the REFLEX II selection function.

2.2 The REFLEX II X-ray luminosity function

As will be described in section 3.2, a key ingredient for the construction of the mock catalogues is the X-ray luminosity function of the REFLEX II sample. We measured the XLF by means of the standard $1/V_{\text{max}}$ estimator (Felten 1977). The resulting X-ray luminosity function, shown by the filled points with error bars in panel (a) of Fig. 1, can be well described by what we call an *extended-Schechter function*:

$$\Phi(L)dL = n_0 \left(\frac{L}{L_*}\right)^{-\alpha} e_q\left(-\frac{L}{L_*}\right) d\left(\frac{L}{L_*}\right). \quad (1)$$

Here n_0 determines the overall normalisation, α characterises the slope of the XLF in the low-luminosity regime and L_* marks the transition from power-law behaviour at low luminosities to the exponential fall-off at high luminosities. The function $e_q(x)$ is the so-called q -exponential distribution (Tsallis 2009), defined as

$$e_q(x) = \begin{cases} e^x & q = 1, \\ (1 + x(1 - q))^{1/(1-q)} & q \neq 1. \end{cases} \quad (2)$$

The best-fitting parameters (n_0, α, L_*, q) to the REFLEX II X-ray luminosity function were determined by implementing a Markov-Chain Monte Carlo (hereafter MCMC) algorithm (e.g Neal 1993). These are $\alpha = 1.54 \pm 0.06$, $L_* = (0.63 \pm 0.15) \times 10^{44} \text{ erg s } h^{-2}$, $n_0 = (4.08 \pm 0.82) \times 10^{-6} (\text{Mpc } h^{-1})^{-3}$, and $q = 1.31 \pm 0.03$, where the quoted errors denote the 68 per cent confidence levels in each parameter. The best fitting extended-Schechter function corresponding to these parameter values is by the dot-dashed line in panel (a) of Fig. 1. Panel (b) of the same figure shows the difference between the measured XLF and the best-fit averaged in the corresponding luminosity bins, in units of the standard deviation. For comparison, in the same panel we show the performance of the Schechter function², showing that such parameterisation cannot fully characterize the REFLEX II XLF, especially at its bright tail.

In order to carry out the statistical analysis using the information of the XLF, we assume a diagonal covariance matrix $C_{ij}^{\Phi} = \sigma_{\Phi}^2(L_i) \delta_{ij}^K$, with a variance given by the Poisson standard deviation $\sigma_{\Phi}(L_i) = \Phi(L_i)/\sqrt{N_i}$, where N_i is the number of clusters in the i -th luminosity bin. This assumption will be also used within the analysis presented in § 3.1, and represents a good description of the covariance matrix of the REFLEX II XLF, as will be shown in § 4.

3 CONSTRUCTION OF THE REFLEX II MOCK CATALOGUES

3.1 The N-body simulations

Our mock catalogues are based on the Low resolution Baryon Acoustic Simulations at ICC (hereafter L-BASICC II) N-body simulations. A detailed description of these simulations can be found in Angulo et al. (2008) and Sánchez et al. (2008). These correspond to 50 realizations of the same flat Λ CDM model characterised by a matter energy-density parameter $\Omega_{\text{mat}} = 0.237$, a baryon energy-density $\Omega_{\text{ba}} = 0.046$, a dimensionless Hubble parameter $h = 0.73$, a rms of mass fluctuations $\sigma_8 = 0.773$ and a scalar spectral index $n_s = 0.997$. Each of the L-BASICC II simulations follows the dark matter distribution using 448³ particles over a comoving box of side $1.34 \text{ Gpc } h^{-1}$, comparable to the Hubble Volume Simulation (Evrard et al. 2002). We used the halo samples at $z = 0$ constructed by means of a friends-of-friends (hereafter FOF) algorithm with a linking length of $b = 0.2$.

Panel (a) of Fig. 2 shows the mean halo mass function

² The best-fitting parameters of the Schechter function ($q = 1$) are $\alpha = 1.71 \pm 0.07$, $L_* = (1.51 \pm 0.15) \times 10^{44} \text{ erg s } h^{-2}$ and $n_0 = (1.29 \pm 0.91) \times 10^{-6} (\text{Mpc } h^{-1})^{-3}$

$n(M)$ from the ensemble of simulations. Due to the resolution of these simulations it is only possible to identify halos with masses $M > 1.7 \times 10^{13} M_{\odot} h^{-1}$ (corresponding to ten dark matter particles), thus probing only the high-mass tail of the halo mass function, which is very well described by the fitting formula of Jenkins et al. (2001) (shown by the solid line in panel (a) of Fig. 2). Note that the cosmological model of the L-BASICC II simulations is slightly different from our fiducial cosmology. We check that the results shown in this paper are not qualitatively modified due to these differences in cosmological parameters (see § 3.5).

Even though the accuracy of the calibration of the parameters in the different recipes for the mass function of dark matter haloes has been pushed to the 5 to 10 per cent level (e.g. Jenkins et al. 2001; Warren et al. 2006; Tinker 2008), it has been shown that the inclusion of baryons in the N-body simulations increases this uncertainty to ~ 15 per cent (Stanek et al. 2009), especially in the mass range probed by the L-BASICC II simulations. Such uncertainties must in principle be taken into account when comparing theoretical predictions with observations on cluster counts/abundances. Although we have not accounted for these uncertainties in the results presented in this paper, we checked that our conclusions do not vary significantly when these are included by allowing up to a 20 per cent uncertainty in the normalisation of halo mass function.

Similarly, it has been shown (e.g. Tinker 2008; Lukić et al. 2009; More et al. 2011) that the FOF halo finder systematically overestimates the masses of dark matter haloes, compared to the masses of the same objects found within simulations at higher resolution. This can be a potential systematic effect that might affect the shape of the scaling relations linking the FOF halo masses to cluster observables, in our case, the X-ray luminosity. Using the recent analysis of More et al. (2011), we have verified that such corrections in the halo masses do not modify our results and conclusions (see § 3.4).

3.2 X-ray luminosity assignment

The first step in the construction of the REFLEX II mock catalogues from the N-body simulations is the assignment of X-ray luminosities to the dark matter halos. We do this following a $M-L_X$ relation which we calibrate in order to reproduce the observed X-ray luminosity function of the REFLEX II sample. The information of the scaling relation $M-L_X$ is encoded in the function $p(L_X|M, z)$, specifying the probability of a cluster to have assigned a X-ray luminosity L_X conditional to its mass M at redshift z . Given the abundance of dark matter haloes $n(M, z)$, the X-ray luminosity function at a given redshift z is given by:

$$\Phi(L_X, z) = \int_0^{\infty} n(M, z) p(L_X|M, z) dM. \quad (3)$$

In this way, given the halo abundance from the N-body simulations, Eq. (3) allows us to calibrate the $M-L_X$ relation in order to reproduce the measured XLF.

Under the assumption of virial and hydrostatic equilibrium, constant gas mass to total mass ratio and thermal bremsstrahlung being the dominant emission mechanism in the intra-cluster medium (see Voit 2005, for a review), the $M-L_X$ relation should be well described by a

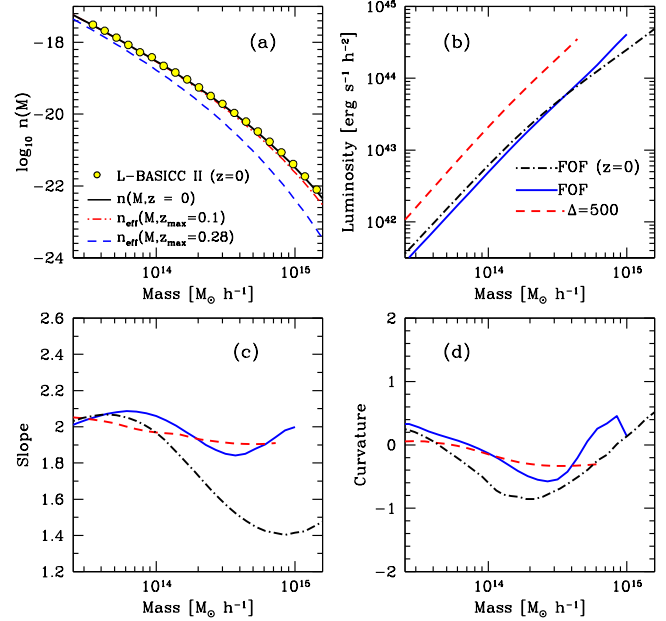


Figure 2. (a) Mean halo mass function $n(M)$ (filled circles) of the L-BASICC II simulations at $z = 0$. The solid line shows the prediction based on the fit of Jenkins et al. (2001). The dotted and dashed lines show the effective mass function derived from a light-cone (following the REFLEX II sensitivity map (see § 3.4)) for two different limiting X-ray luminosities. (b) $M-L_X$ relation obtained from the abundance matching technique using the mass function at $z = 0$ (dot-dashed line), and light-cone estimates using the FOF (solid line) and SO haloes with $\Delta = 500$ (see § 3.4). (c) Slope (first derivative) of the $M-L_X$ relation. (d) Curvature (second derivative) of the $M-L_X$ relation.

power-law, at least for the brightest galaxy clusters (e.g. Reiprich & Böhringer 1999; Stanek et al. 2006; Maughan 2007; Rykoff et al. 2008; Pratt et al. 2009; Vikhlinin et al. 2009). Furthermore, within the *ROSAT* energy band, the X-ray emissivity is weakly dependent on the temperature of the gas, specially for the hot clusters ($T \geq 3$ keV or $L_X \gtrsim L_{\star}$). These facts can be shown to generate scaling relations of the form $L_X \propto M_{\text{vir}}$ and $L_X^{\text{bol}} \propto M_{\text{vir}}^{4/3}$ for band and bolometric luminosities respectively. Deviations from self-similar expectations are associated with non-thermal processes such as AGN feedback from the growth of super-massive black-holes (e.g. Borgani et al. 2005; Kay et al. 2007; Puchwein et al. 2008; Stanek et al. 2010; Short et al. 2010). These feedback processes lead to a more significant gas depletion for low mass systems, reducing the X-ray luminosity and breaking the simple self-similarity as a function of mass. The evolution of the $M-L_X$ relation has been studied in observations (e.g. Vikhlinin et al. 2009; Reichert et al. 2011) and found to also show deviations from the simple self-similar model.

A simple non-parametric estimate of the underlying $M-L_X$ relation can be obtained by implementing the so-called abundance matching technique (e.g. Behroozi et al. 2010), in which we determine the X-ray luminosity $\bar{L}_X(M)$ as a function of the halo mass by matching the cumulative abundances $\int_{L_X}^{\infty} \Phi(L') dL' = \int_M^{\infty} n(M') dM'$. This method is applicable under the assumption that X-ray luminosity is a monotonically increasing function of the halo mass with no intrinsic scatter. The resulting $M-L_X$ relation is shown by

the black dot-dashed line in panel (b) of Fig. 2, displaying deviations from a power-law. To obtain this result we used the recipe for the halo mass function of Jenkins et al. (2001) computed for the cosmological model of the L-BASICC II simulations at $z = 0$.

In order to quantify the inferred departure from a power-law M - L_X relation, the dot-dashed lines in panels (c) and (d) of Fig. 2 show the behaviour of its first and second derivatives, respectively, as a function of the halo mass. Within the luminosity range explored by the REFLEX II X-ray luminosity function, the slope of the M - L_X relation displays a transition from a maximum value of approximately ~ 2 at $\sim 5 \times 10^{13} M_\odot h^{-1}$ to ~ 1.4 at a mass scale of $\sim 10^{15} M_\odot h^{-1}$. Accordingly, the curvature displays positive values in the low halo mass regime $M \lesssim 10^{13.5} M_\odot h^{-1}$. In the intermediate halo mass range $5 \times 10^{13} \lesssim M \lesssim 10^{15} M_\odot h^{-1}$, the curvature displays negative values and resume positive values for the high-mass haloes. Although these results are based on a simple halo abundance matching technique which ignores relevant physical effects, they suggest that a simple power-law relation M - L_X will not be enough to describe the observed XLF through Eq. (3).

We calibrate the M - L_X relation that we use in the construction of our mock catalogues directly from the halo samples in the N-body simulations. We assume that X-ray luminosities are distributed around a mean scaling relation with a log-normal scatter in the luminosity (at a fixed mass) $\sigma_{\ln L|M}$. In order to account for the deviation from a power-law as suggested by the abundance matching technique, we adopted a mass-dependent slope (or running-index scaling-law) to parameterise the mean M - L_X relation in the whole luminosity range covered by the REFLEX II sample. Defining $\bar{\ell} \equiv \log_{10}(\bar{L}_X/10^{44} \text{ erg s}^{-1} h^{-2})$ and $m \equiv \log_{10}(M/10^{14} M_\odot h^{-1})$, our input mean scaling relation M - L_X has the form

$$\bar{\ell}(m) = a + bm + cm^2, \quad (4)$$

where a determines the mean luminosity at $10^{14} M_\odot h^{-1}$, b determines the slope at that mass-scale and the parameter c characterises the curvature. We assigned X-ray luminosities to the dark matter haloes using Eq. (4), applying a log-normal scatter around $\ln \bar{L}_X$ characterised by $\sigma_{\ln L|M} = 0.26$ (~ 30 per cent scatter). This value was derived by Stanek et al. (2006) based on cluster number counts and spatial clustering measured from a sub-sample of the REFLEX catalogue. We note however that such a value was determined under the assumption of a power-law scaling relation. Furthermore, in their analysis, Stanek et al. (2006) assumed a fiducial cosmological model with $\Omega_{\text{mat}} = 0.24$ and a power spectrum normalisation of $\sigma_8 = 0.85$, which is higher than our fiducial value $\sigma_8 = 0.773$. Reiprich (2006) verified that the high intrinsic scatter measured by Stanek et al. (2006) was related to the cosmological model they implemented, mainly, to the high value of σ_8 . Using the cosmological parameters derived from WMAP-3year data (Spergel et al. 2007), Reiprich (2006) found that a small intrinsic scatter was still able to describe the observations (within the mass uncertainties). Mantz et al. (2010) used a fiducial cosmological model similar to ours, and found a larger scatter (~ 40 per cent), though it was substantially reduced (~ 6 per cent) when core-excised clusters were used in their analysis. We therefore emphasise that the param-

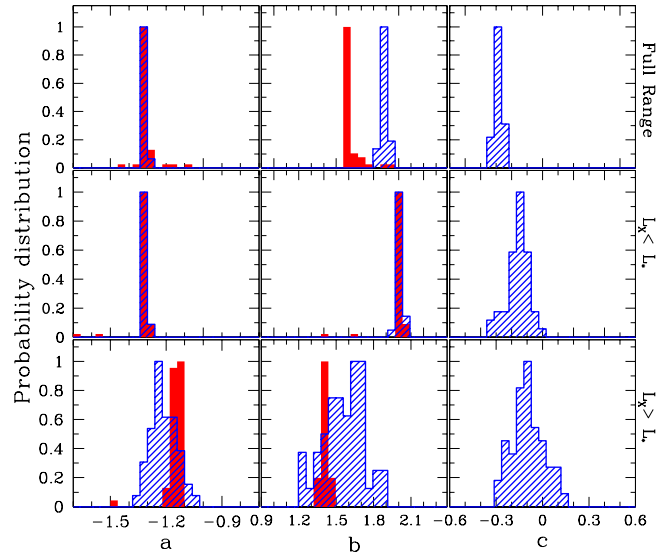


Figure 3. Distribution of the best-fitting parameters (a, b, c) determined from the 50 realizations of the L-BASICC II simulations within the full luminosity range as well as in the faint and bright tail of the XLF. Solid line distributions show the results assuming a M - L_X relation given by Eq. (4). Filled histograms show the distribution of parameters associated with a power-law ($c = 0$).

eters of the M - L_X relation obtained with a fixed scatter and from a FOF halo mass function *are only meant to reproduce the cluster abundance within the N-body simulations and $z = 0$.*

On top of the intrinsic scatter, we introduced the errors in the X-ray luminosity through a second log-normal scatter with $\sigma = 0.2$. These two scatters can be added in quadrature, such that the total M - L_X relation preserves a log-normal scatter given by $\tilde{\sigma} = 0.328$ (39 per cent scatter). After luminosities were assigned to each halo we determined the luminosity functions within the 50 simulation boxes. We implemented a MCMC algorithm to determine the set of parameters (a, b, c) in Eq. (4) by comparing the obtained luminosity distributions with the measured REFLEX II XLF, assuming a Poisson-noise standard deviation, as pointed out in § 2.2.

As a consistency check, we have verified that replacing the measured XLF by the best fit extended-Schechter function of Eq. (1) yields a set of parameters (a, b, c) different by less than 5 per cent.

3.3 The inferred M - L_X relation

Following the procedure described in § 3.2, we obtained best-fitting values of the parameters (a, b, c) from each of the 50 L-BASICC II realizations. The distributions of these values are shown in the upper panels of Fig. 3, and present narrow peaks around the values $a = -1.36 \pm 0.03$, $b = 1.88 \pm 0.05$ and $c = -0.29 \pm 0.04$ (where the errors represent the variance from the ensemble of simulations). These values, together with the effective scatter $\tilde{\sigma} = 0.328$, were used in the final construction of the mock catalogues described in § 3.5 and used in Paper I. The constraints on c indicate a $\sim 7\sigma$ deviation from the power-law M - L_X relation (i.e. $c = 0$). The solid line in Fig. 4 shows the mean M - L_X relation obtained

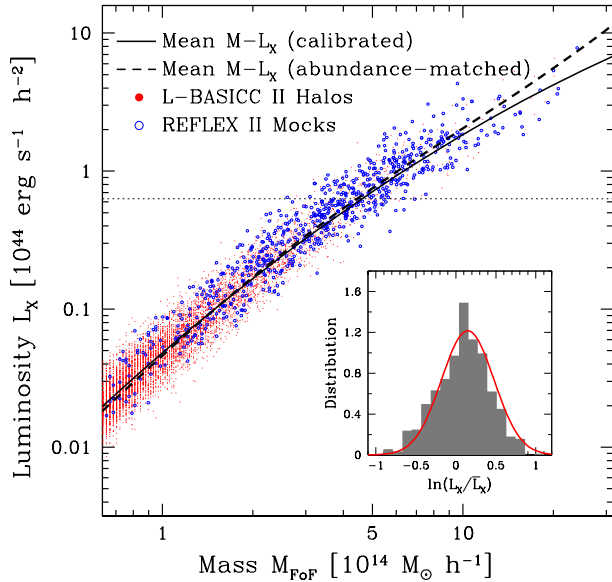


Figure 4. M - L_X relation of the REFLEX II mock catalogues. The solid line represents the mean M - L_X relation calibrated from $\Phi(L_X)$. Filled circles correspond to individual halos in one of the L-BASICC II simulations with X-ray luminosities assigned as described in § 3.5). Open circles correspond to mock clusters in one member of the ensemble of 100 REFLEX II mock catalogue. The dashed line represents the M - L_X relation determined by the abundance matching technique (§ 3.5). The horizontal line marks the value L_* . The inner plot shows the distribution of the luminosities with respect to their mean value. The solid line represents a Gaussian distribution with dispersion $\bar{\sigma}$ centred at $\ln(L/\bar{L}) = (d \ln V/d \ln L) \bar{\sigma}^2 \sim 0.14$, where $V(L)$ is the volume as a function of the X-ray luminosity (see § 4.1).

with these set of parameters. The points correspond to individual halos in one of the L-BASICC II realizations with X-ray luminosities assigned following our M - L_X relation, while open circles represent clusters in one of our final REFLEX II mock catalogues (i.e, once the REFLEX II selection function is applied as described in § 3.5). As shown by the solid histogram in Fig. 1, the luminosity distribution generated through this calibration provides an excellent match to the measured X-ray luminosity function of the REFLEX II sample.

The M - L_X relation obtained through this calibration procedure is in agreement with that derived from the simple abundance matching technique described in § 2.2 (shown by the dashed line in Fig. 4), especially for $M \lesssim 5 \times 10^{14} M_\odot h^{-1}$ which corresponds to a luminosity $L_X \sim L_*$. At higher masses, the difference between the two is clear. Due to the exponential fall-off of the halo mass function at such high mass scales, the obtained X-ray luminosity distribution of the halos is very sensitive to the assumed scatter in the M - L_X relation.

As a consistency check, we have verified that the values (a, b, c) obtained from the resulting distribution within the L-BASICC II simulations are in good agreement with those obtained when the fitting formulae of Jenkins et al. (2001) is used to compare the measured $\Phi(L_X)$ against the prediction from Eq. (3). The results obtained in this case are $a = -1.29 \pm 0.04$, $b = 1.95 \pm 0.09$ and $c = -0.31 \pm 0.06$, where the errors denote the 1σ confidence intervals.

A power-law scaling relation could still be sufficient to reproduce the abundance of high luminosity ($L_X > L_*$) galaxy clusters. In order to verify this, we repeated the procedure described in § 3.2 to calibrated the M - L_X relation in the faint ($L_X \leq L_*$) and bright ($L_X > L_*$) tails of the luminosity function. The results are shown in the second and third rows of Fig.3. The set of parameters calibrated in the first interval ($L_X < L_*$) are marginally compatible with a power-law (for instance ~ 6 per cent of the realizations displayed curvatures in the range $|c| \leq 0.05$), whereas the analysis derived from the bright tail is more consistent with such scaling relation (~ 25 percent of the realizations had $|c| \leq 0.05$). We have checked that by pushing the limiting luminosity up to higher values, the resulting distribution of the curvature is well peaked at the value $c \sim 0$, though the distribution becomes wider due to the low number of objects with such luminosities. Fig. 3 also shows the distribution of the parameters associated with a power-law M - L_X relation, using the full range as well as the faint and bright end tails of the luminosity distribution. The evident shifts in the peaking values of the slope b in these two luminosity ranges shows the need for a mass-dependent slope, or in general, for deviations from a power-law M - L_X relation in case the full luminosity range is used in the analysis.

3.4 On the shape of the M - L_X scaling relation

As discussed in § 2, the determination of the X-ray luminosities of the REFLEX II sample assumed, among other things, a fiducial set of cosmological parameters and a definition of halo masses, namely, SO masses with $\Delta = 500$. In this subsection we briefly explore the possible impact of the differences between these fiducial values and the corresponding quantities characterising the L-BASICC II N-body simulations, on the recovered values of the parameters of the M - L_X relation.

- *Resolution effects.* It has been shown (e.g Warren et al. 2006; Lukić et al. 2009; More et al. 2011) that the finite number of particles defining a dark matter halo is overestimated by the FOF finder algorithm, when compared to the same masses obtained with simulations of higher resolution. In particular, the empirical correction of Warren et al. (2006), based on the number of particles defining a dark matter halo, was designed to match the abundance of low resolution to that of higher resolution simulations. This correction leads to a 40 per cent mass overestimation at the resolution limit of the L-BASICC II simulations, reducing to a few percent at $10^{15} M_\odot h^{-1}$. Based on percolation theory, this systematic effect has been modeled by More et al. (2011), who showed that the FOF masses are overestimated by ~ 30 per cent at the resolution of the L-BASICC II simulations, and by 15 per cent at a mass scale of $10^{15} M_\odot h^{-1}$ (S. More, private communication), representing a higher correction than that of Warren et al. (2006). In order to check the impact of this systematic effect on our results, we corrected the halo masses within the L-BASICC II simulations and re-calibrated the scaling relation given by Eq. (4) on a number of realizations. The results show a 15 per cent increment in the normalization a , with its corresponding decrease the slope b (around 10 per cent) and a shift of the curvature c towards positive values (around 15 per cent), with respect to

		<i>a</i>	<i>b</i>	<i>c</i>
i	FOF L-BASICC II Simulation	-1.36 ± 0.03	1.88 ± 0.05	-0.29 ± 0.04
ii	FOF L-BASICC II Simulation: masses corrected	-1.10 ± 0.02	1.70 ± 0.04	-0.23 ± 0.04
iii	FOF (Jenkins et al. 2001)	-1.29 ± 0.04	1.95 ± 0.09	-0.31 ± 0.06
iv	SO $\Delta = 500$ (Tinker 2008) full L_X range	-0.68 ± 0.06	1.65 ± 0.03	-0.38 ± 0.04
v	SO $\Delta = 500$ (Tinker 2008) $L > 1.6L_*$	-0.69 ± 0.07	1.45 ± 0.26	-0.15 ± 0.22
vi	SO $\Delta = 500$ (Tinker 2008) $L > 1.6L_*$, power-law	-0.64 ± 0.03	1.27 ± 0.05	0

Table 1. Parameters of the M - L_X relation in Eq. (4) obtained by calibration against the observed REFLEX II XLF: i) using the L-BASICC II simulations, ii) using the L-BASICC II simulations with FOF masses corrected as More et al. (2011), iii) using the Jenkins et al. (2001) fitting formula for the halo mass function, and iv) & v) using the Tinker (2008) mass function for SO masses with $\Delta = 500$ in two luminosity intervals. In order to compare with the analysis of Mantz et al. (2010), the last row vi) shows the results obtained by fitting a power-law in the range $L > 1.6L_*$.

our original estimations. In particular, the shift in the curvature corresponds to approximately 1σ , excluding the value $c = 0$ with a statistical significance of $\sim 4\sigma$. We can conclude that the correction for the finite number of particles in some extent diminishes the departure from a power-law scaling relation, although not completely.

- *Cosmological parameters.* We have tested the impact of the cosmological parameters in the calibration of the scaling relation, by constraining the set (a, b, c) using the Jenkins et al. (2001) mass function at $z = 0$ computed for different values of Ω_{mat} in the range $0.15 - 0.35$, keeping both σ_8 fixed to our fiducial value or letting it vary as $\sigma_8 = 0.45\Omega_{\text{mat}}^{-0.3}$ (e.g. Evrard et al. 2002). In both cases, while the amplitude a (the slope b) decreases (increases) with respect to Ω_{mat} , the curvature c remains approximately constant, $c \neq 0$ with a 2σ significance.

- *Redshift evolution.* The redshift evolution of the mean matter density of the Universe can be imprinted in the amplitude of the M - L_X relation (e.g. Borgani 2001; Voit 2005). The parameterisation given by Eq. (4) can then be thought of as accounting for such evolution through the conversion $A(z) \rightarrow 10^a M^{cm}$, in case the true underlying M - L_X relation is given by a power-law $L_X = A(z)M^b$. On the other hand, even without a redshift dependent amplitude (i.e. $A(z)$ constant), the function $p(L_X|M, z)$ could still evolve with redshift through its intrinsic scatter (e.g. Fabjan et al. 2011). For the purposes of building mock catalogues from a snapshot of the simulations, such dependency could be translated to a mass-dependent scatter. We explored this possibility by calibrating a power-law M - L_X relation with a scatter given by $\sigma(M) = \sigma_{\text{inL|M}}(M/10^{14} M_\odot h^{-1})^\gamma$. The resulting X-ray luminosity distribution generated by this parameterisation (with best-fitting values $a \sim -1.2$, $b \sim 1.8$ and $\gamma \sim -2.3$ with ~ 50 per cent error in γ) is shown by the dot-dashed histogram in Fig. 1. Such parameterisation represents a mild improvement with respect to the power-law or running index M - L_X relation in the bright end ($L > L_*$) of the XLF, while working as good as the power-law for $L \lesssim L_*$ clusters.

- *Light-cone effects.* In order to take into account the redshift evolution of the halo abundance, the XLF measured within a past light-cone must be compared with the volume average of Eq. (3). Under the assumption of a redshift-independent M - L_X relation, we can write the prediction for the luminosity functions in the light-cone as

$$\Phi(L_X) = \int_0^\infty n_{\text{eff}}(M, z_{\text{max}}) p(L_X|M) dM, \quad (5)$$

where $n_{\text{eff}}(M, z_{\text{max}})$ is the halo mass function averaged over the volume of the light-cone defined by the sample:

$$n_{\text{eff}}(M, z_{\text{max}}) = \frac{1}{V(z_{\text{max}})} \int_{V(z_{\text{max}})} n(M, z) \frac{dV}{dz} dz, \quad (6)$$

with $z_{\text{max}} = z_{\text{max}}(L_X)$ as the maximum redshift allowed for a cluster with luminosity L_X in order to be detected, and $V(z_{\text{max}})$ is the comoving volume at that redshift. This information is encoded in the REFLEX II sensitivity map described in § 2.1. As an example, we show the behaviour of $n_{\text{eff}}(M, z_{\text{max}})$ in panel (a) of Fig. 2, based on the halo mass function for FOF and SO masses. In order to apply the match abundance technique to derive an estimate of the shape of the M - L_X relation using Eq. (6), we carried out an iterative process in which an initial power-law scaling relation was assumed, $\ell = -1.0 + 1.5m$, from which $n_{\text{eff}}(M, z_{\text{max}}(M))$ could be determined in order to match the abundances, leading to a new estimation of the M - L_X relation, which is used as an input for the next iteration. The resulting M - L_X relations (convergence is achieved after few iterations) derived from the FOF and SO mass functions are shown in panel (b) of Fig. 2, with its first and second derivatives in panels (c) and (d) respectively. The recovered scaling relation still displays departures from a power-law, although the curvature is slightly smaller than that derived from the simulation snapshots (dot-dashed line in Fig. 2). The deviation from a power-law is more evident for FOF masses than for SO masses. This might indicate that the deviations from a power-law scaling relation observed by matching the abundances at redshift $z = 0$ are not significantly accounted for by the evolution of the halo-abundance within the light cone defined by the REFLEX II sample, at least in the case of vanishing intrinsic scatter.

- *Definition of halo mass.* We calibrated the M - L_X relation given by Eq. (4) using the fitting formulae of Tinker (2008) for SO haloes with $\Delta = 500$. The mass function was evaluated at the median redshift of the sample $\bar{z} \approx 0.09$. Fixing the intrinsic scatter to our fiducial value we obtained $a = -0.68 \pm 0.06$, $b = 1.65 \pm 0.03$ and $c = -0.38 \pm 0.04$. The value for the curvature excludes the power-law scaling relation with $\sim 7\sigma$ confidence. Similarly, for clusters with $L_X > L_*$ (with a median redshift of $\bar{z} \approx 0.14$) we found $a = -0.73 \pm 0.02$, $b = 1.68 \pm 0.16$, and $c = -0.34 \pm 0.14$, excluding the power-law behavior to $\sim 2\sigma$ significance. We calibrated a power-law scaling relation in the range $L_X > 1.6L_* \approx 10^{44} \text{erg s}^{-1} h^{-2}$, similar to that

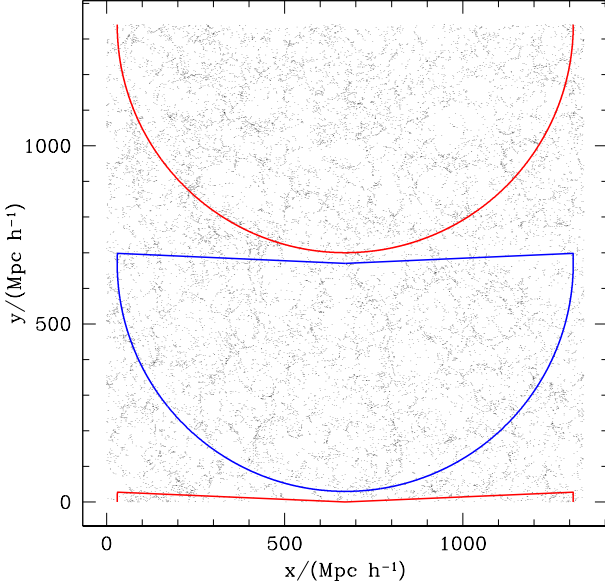


Figure 5. Slice of $100 \text{ Mpc } h^{-1}$ width through the centre of the halo distribution in one of the L-BASICC II simulations. The solid lines indicate the geometric configuration used to extract two independent mock catalogues with $z_{\text{max}} = 0.22$ from each realization.

used by Mantz et al. (2010), obtaining $a = -0.64 \pm 0.05$ and $b = 1.27 \pm 0.05$, in good agreement with that analysis. In the same range, the fit to Eq. (4) yields a curvature of $c = -0.15 \pm 0.23$, compatible with a power-law.

The tests presented in this section show that the deviation from a power-law scaling relation in the full X-ray luminosity range probed by the REFLEX II XLF is likely not due to differences in the mass definition, the cosmological parameters or evolution along the light cone. This is nevertheless not conclusive, in the sense that a full analysis including the evolution of the scaling relation, its intrinsic scatter and the uncertainties in the halo abundance is still required in order to draw stronger conclusions about the cluster scaling relations.

Table 1 summarizes the values of the parameters (a, b, c) obtained from the various analysis presented in this section.

3.5 The construction of the mock catalogues

We now describe the procedure followed to construct the REFLEX II mock catalogues. First, we note that in Paper I it was shown that the effective volume for clustering analyses (e.g. Feldman et al. 1994) probed by the REFLEX II sample does not increase substantially beyond redshift $z \approx 0.22$. As the primary goal of the set of mock catalogues is to determine covariance matrices for the statistical analysis of the large-scale structure probed by the REFLEX II sample, we set this value as the maximum redshift of the mock catalogues. This in turn allowed us to construct 100 independent mock catalogues out of the 50 L-BASICC II realizations. Mock catalogues with higher maximum redshifts can in principle be constructed, at the cost of having less independent realizations.

The geometric arrangement of the mock catalogues is

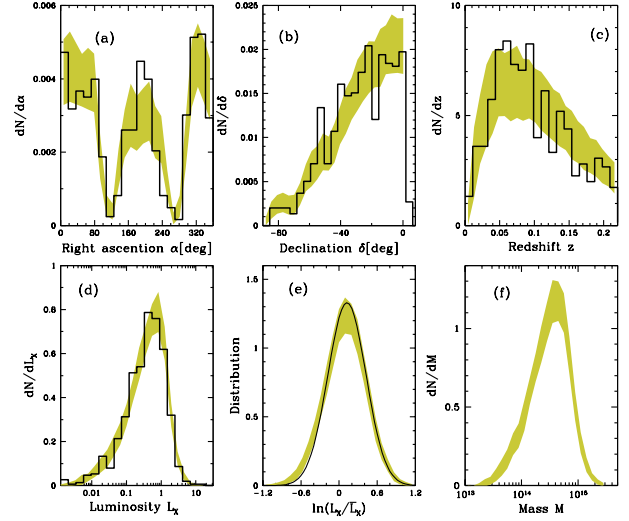


Figure 6. Properties of the mock catalogues: (a) right-ascension, (b) declination, (c) redshift (d) luminosity (e) luminosity relative to the true underlying $M-L_X$ relation and (f) mass distribution. The shaded areas show the standard deviation in the distribution of each property derived from the set of mock catalogues and compared to the corresponding property in the REFLEX II sample (solid line). In panel (f) the solid line shows a Gaussian distribution centred at $\delta\sigma^2$ (see § 4.1)

depicted in Fig. 5, where a slice cut of $100 h^{-1} \text{ Mpc}$ through the center of one of the L-BASICC II realizations is shown. Given such geometric arrangement, we assigned a cosmological redshift z_{cos} to each halo by inverting the redshift-comoving distance relation $r(z_{\text{cos}}) = \int_0^{z_{\text{cos}}} dz' H^{-1}(z')$ for the cosmology of the simulations. The final redshifts of the halos were obtained taking into account the distortions introduced by their peculiar velocities v as $z = (1 + z_{\text{cos}})(1 + z_{\text{pec}}) - 1$, where $z_{\text{pec}} = v/H_0$. For the $z = 0$ output of the L-BASICC II simulations, the distribution of peculiar velocities displays a mean value of $\bar{v} \approx 350 \text{ km s}^{-1}$ with a velocity dispersion of $\sigma \approx 180 \text{ km s}^{-1}$, which in terms of redshift corresponds to $\Delta z \sim 6 \times 10^{-4}$. As can be seen in table 2 of Guzzo et al. (2009), the redshift distortions induced by spectroscopic redshift uncertainties in the REFLEX II sample are significantly smaller than those induced by peculiar velocities. Therefore we do not introduce such effect in the estimate of the redshift of our mock clusters.

We assigned X-ray luminosities to the dark matter haloes according to the $M-L_X$ relation described in § 3.3. These halos are then *observed* through the REFLEX II sensitivity map, rejecting those haloes with luminosities below the limiting luminosity L_X^{lim} at a given location. The open circles in Fig. 4 correspond to individual objects in one of our final REFLEX II mock catalogues which, with a minimum mass $M \sim 3.5 \times 10^{13} h^{-1} M_{\odot}$, corresponding to a 20 particle dark matter halo, covers a mass range well within the resolution limit of the simulations.

4 PROPERTIES OF THE REFLEX II MOCK CATALOGUES

In this section we discuss some of the most relevant properties of the REFLEX II mock catalogues.

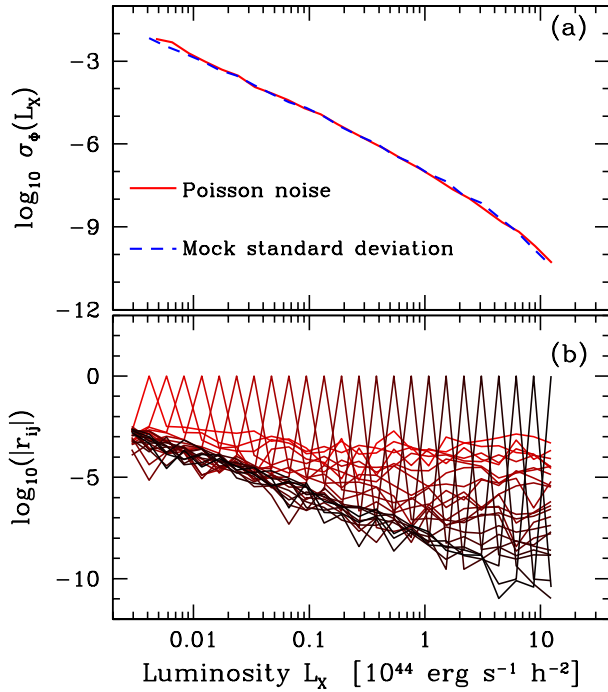


Figure 7. Covariance matrix of the XLF. Panel (a) shows the comparison between the standard deviation of the XLF derived from the set of mock catalogues, and the Poisson-noise prediction determined from the number of clusters in each bin of X-ray luminosity. Panel (b) shows the correlation coefficients r_{ij} of the XLF.

4.1 Basic properties

The underlying M - L_X relation applied to construct the REFLEX II mock catalogues (and used in the clustering analysis of Paper I) is characterised by Eq. (4), with the set of parameters shown in § 3.3. The performance of the REFLEX II sky-mask is shown in panels (a) and (b) of Fig. 6 by means of the distribution in equatorial coordinates of the mock catalogues, compared to that of the REFLEX II sample, shown by the solid line. The Milky-way band is well described in panel (a) by the two minimum distribution values at $\alpha \sim 100$ and $\alpha \sim 250$ deg (see also fig. 1 of Paper I). Panels (c) and (d) show respectively the redshift and X-ray luminosity distributions, displaying good agreement with that of the real REFLEX II sample. The mass distribution within the mock catalogues is shown in panel (f) of Fig. 6. This implies an average halo mass of $M \simeq 4 \times 10^{14} h^{-1} M_\odot$ for the REFLEX II clusters.

The application of the REFLEX II selection function to the N-body simulations, introduces in our set of mock catalogues a selection effect inherent to all flux-limited samples, namely, the fact that objects with increasing luminosities probe larger cosmological volumes. In combination with the intrinsic scatter in the M - L_X relation this introduces the so-called Malmquist bias which, if unaccounted for, can lead to biased estimates of the underlying scaling relation, especially when a threshold in luminosity is imposed to the sample. Our set of mock catalogues can then be used as a control sample to test different methods to obtain scaling relations taking into account the selection effects mentioned above. At a given mass M the Malmquist bias causes the mean

observed M - L_X relation $\langle L(M) \rangle$ to deviate from the underlying M - L_X relation $\bar{L}(M)$ according to (e.g Stanek et al. 2006; Vikhlinin et al. 2009; Pratt et al. 2009)

$$\langle \ln L_X \rangle = \ln \bar{L}_X(M) + \delta \tilde{\sigma}^2, \quad (7)$$

where it is assumed that the volume probed by a cluster of luminosity L_X scales as $V(L_X) \propto L_X^\delta$ ($\delta = 0$ for a volume limited sample) together with a log-normal distribution function $p(L_X|M, z)$ with scatter $\tilde{\sigma}$. Under the assumption of a non-evolving M - L_X relation, the Malmquist bias can be translated into an overestimation of the slope and an underestimation of the amplitude in the M - L_X relation (e.g Reiprich & Böhringer 1999). In panel (e) of Fig. 6 we show the distribution of luminosities around the mean M - L_X relation given by Eq. (4), for the 100 mock catalogues. The dashed line represents a log-normal distribution centred at $\ln(L/\bar{L}) = \delta \tilde{\sigma}^2 \approx 0.14$, where we have used $\delta = 1.38$, which gives a good description of the maximum volume as a function of the X-ray luminosity. In terms of luminosities, this bias is translated into a factor ~ 1.15 .

We finally study the behavior of the covariance matrix of the REFLEX II XLF. In panel (a) of Fig. 7 we compare the standard deviation obtained from the final set of mock catalogues with that derived from a Poisson noise. The good agreement between these two estimates implies that the inhomogeneous spatial distribution of X-ray galaxy clusters (i.e, the sampling variance) has a minor impact on the determination of the variance of the XLF (e.g Smith 2012) given the comoving volume and luminosity range probed by the REFLEX II sample. Furthermore, we verified that the off-diagonal elements of the covariance matrix of the XLF are negligible compared to the variance. In this regard, panel (b) of Fig. 7 shows the correlation coefficients defined by $|r_{ij}| \equiv |C_{ij}^\Phi| / \sqrt{C_{ii}^\Phi C_{jj}^\Phi}$ determined from the suite of mock catalogues, showing in general weak correlations between different luminosity bins, ranging from $r_{ij} \sim 10^{-3}$ at low luminosities to $r_{ij} \sim 10^{-10}$ at high luminosities. A more detailed analysis of the REFLEX II XLF will be presented in a forthcoming paper (Böhringer et al., in preparation).

4.2 Clustering properties

The power spectra of the REFLEX II mock catalogues were analysed in Paper I. These measurements were obtained following the method described in Paper I, based on the minimal-variance estimator of Feldman et al. (1994). This study showed that the mean power spectra from our ensemble of mocks catalogues for different limiting luminosities is in excellent agreement with those of the REFLEX II sample on intermediate and large scales ($0.02 < k/(h \text{ Mpc}^{-1}) < 0.3$). While a detailed analysis of the clustering in configuration space will be presented in a forthcoming paper (Sánchez et al., in preparation), also in this case we find good agreement between the clustering signal of the REFLEX II sample and that of the mock catalogues. This allows us to use our mock catalogues for its main application in the context of large scale structure, that is, to obtain estimates of the covariance matrices of these measurements.

Paper I presented an analysis of the bin-averaged covariance matrix $\hat{C}(k_i, k_j)$ of the cluster power spectrum. This covariance matrix showed highly correlated modes (with

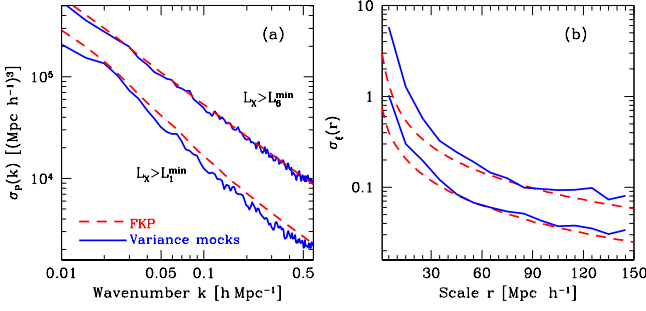


Figure 8. Variance of the power spectrum (panel a) and the correlation function (panel b) measured from the mock catalogues (solid lines) compared with the prediction from the estimator of Feldman et al. (1994) (dashed lines), for two values of minimum X-ray luminosity.

correlation coefficients $r_{ij} > 0.9$) on intermediate ($k \sim 0.08h \text{ Mpc}^{-1}$) and small scales ($k \sim 0.3h \text{ Mpc}^{-1}$), mostly due to mode coupling induced by the survey window function. Feldman et al. (1994) derived an approximated expression for the variance of the spherically averaged power spectrum under the assumption of Gaussian-distributed power around the true underlying value, given by:

$$\frac{\sigma_P^2(k)}{P(k)^2} = \frac{2}{V_k V_{\text{eff}}(k)}, \quad (8)$$

where $V_k \approx 4\pi k^2 \delta k / (2\pi)^3$ is the volume of a spherical shell of width δk and $V_{\text{eff}}(k)$ is the effective (coherence) volume probed by the survey at a scale k (e.g. Feldman et al. 1994). In its simpler form (for a volume limited sample), this contains the contribution from cosmic variance and shot-noise. The prediction of Eq. (8) can easily be translated into the variance of the two-point correlation function as (Cohn 2006; Smith et al. 2008; Sánchez et al. 2008):

$$\sigma_\xi^2(r) = \frac{1}{2\pi^2} \int_0^\infty dk k^2 j_0(kr)^2 \sigma_P^2(k), \quad (9)$$

where $j_0(y)$ is the zero-th order spherical Bessel function.

Panel (a) of Fig. 8 compares the variance of the cluster power spectrum derived from the set of mock catalogues using sub-samples with minimum luminosities $L_1^{\text{min}} = 0.049$ and $L_6^{\text{min}} = 0.588 \times 10^{44} \text{ erg s}^{-1} h^{-2}$ against the prediction of Eq. (8). Similarly, panel (b) of the same figure shows the behaviour of the variance of the cluster correlation function for the same values of minimum X-ray luminosity. Despite its simplicity, Eq. (8) gives a good account of the variances inferred from our mock catalogues. However, significant differences exist, especially for the small-scale σ_ξ , which highlight the importance of the ensemble of mock catalogues as a tool to obtain accurate estimations of covariance matrices which take into account the full effect of non-linearities.

Our ensemble of mock catalogues allows us to test another common assumption when comparing clustering measurements against the predictions of cosmological models, that of a Gaussian likelihood function. By studying the distribution function of the values of $P(k)$ and $\xi(s)$ obtained from the mocks it is possible to reconstruct the shape of the likelihood function and find deviations from the simple Gaussian assumption. As the covariance matrices for these statistics are not diagonal, this analysis is simplified by working on their “de-correlated” versions λ_i and ζ_i defined

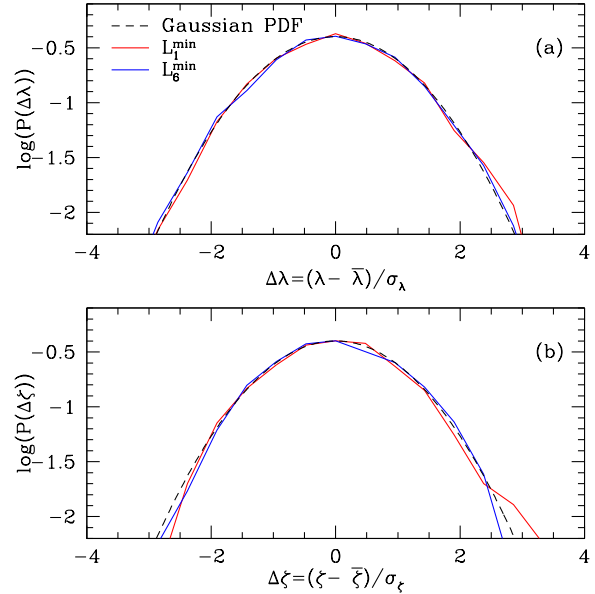


Figure 9. Probability distribution function (PDF) of the values of the power spectra (panel a) and correlation functions (panel b) in our ensemble of mock catalogues for two values of minimum X-ray luminosity. The dashed lines represent a Gaussian PDF.

as:

$$\lambda_i = (M_P^{-1})_{ij} P_j, \quad (10)$$

$$\zeta_i = (M_\xi^{-1})_{ij} \xi_j, \quad (11)$$

where M_P and M_ξ are the transformation matrices of the basis where the covariance matrices C_P and C_ξ are diagonal (given by their eigenvectors). Fig. 9 shows the probability distribution function of $\Delta\lambda = (\lambda_i - \bar{\lambda}_i)/\sigma_\lambda$ and $\Delta\zeta = (\zeta_i - \bar{\zeta}_i)/\sigma_\zeta$ for two limiting luminosities for the power spectrum (panel a) and correlation function (panel b). These are well described by the prediction for a Gaussian distribution, shown by the dashed line, indicating that deviations from the Gaussian case are very small.

Fig. 10 shows the distribution of the chi-squared values χ^2 associated with the cluster power spectrum and the correlation function within the 100 mock catalogues, computed with respect to their mean values within the ensemble. The observed distributions are well described by a χ^2 distribution (Abramowitz & Stegun 1972) shown by the dashed lines, computed using the number of modes in each scale interval shown in the figure. This implies that the distribution of these quantities at a fixed scale is likely to follow a Gaussian distribution. We have tested this by performing a Kolmogorov-Smirnov test (e.g. Press et al. 2002), assuming as a null hypothesis a Gaussian distribution for the quantity $(\hat{P}(k_i) - \bar{P}(k_i))/\bar{P}(k_i)$, with zero mean and dispersion $\sigma(k_i)/\bar{P}(k_i)$. The test shows that on scales $0.02 < k_i/(h \text{ Mpc}^{-1}) \lesssim 0.2$ the distribution is compatible with the null-hypothesis to a $\gtrsim 88$ per cent level. We can therefore conclude that the resulting covariance matrix of the REFLEX II power spectrum can be used in an error analysis based on the assumption of Gaussian likelihoods. Similar conclusions can be obtained with respect to the clustering in configuration space.

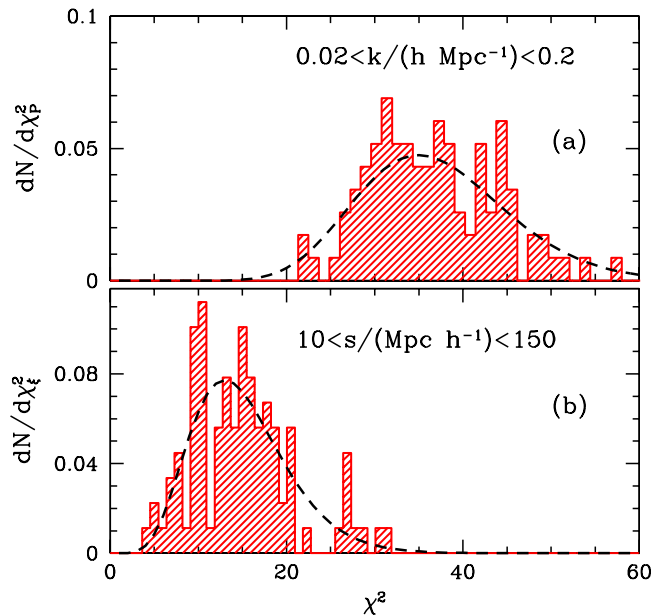


Figure 10. Distribution of the χ^2 values associated to the power spectrum (panel (a)) and the correlation function (panel (b)) of the 100 mock catalogues computed with respect to the mean of the ensemble. The dashed line represents the χ^2 distribution for the corresponding number of modes in each interval of scales or wavenumbers.

5 CONCLUSIONS

In this paper we describe the procedure to construct a suite of galaxy cluster mock catalogues based on the X-ray luminosity function $\Phi(L_X)$ of the REFLEX II sample and dark matter halo samples identified in the L-BASICC II N-body simulations.

The construction of our mock catalogues relies on the scaling relation between halo masses and X-ray luminosity in the *ROSAT* energy band. Given the fact that the abundance of galaxy clusters is highly sensitive to the underlying scaling relation, we calibrate our mass proxy based on the X-ray luminosity function of the REFLEX II sample and the halo-abundance of the N-body simulations. We find that in the luminosity range probed by the REFLEX II sample, the observed $\Phi(L_X)$ demands a $M-L_X$ relation that deviates from a power-law.

We qualitatively discarded such behaviour as a by-product of the differences between the features of the N-body simulations and the assumptions under which the REFLEX II catalogue was built, namely, the definition of halo masses and the cosmological parameters. Similarly, the deviations from a power-law are likely not associated with possible light-cone effects (at least under the assumption of negligible intrinsic scatter). However, we find that a power-law is still sufficient to generate the observed abundance for bright clusters ($L_X \geq 10^{44} \text{ erg s h}^{-2}$), in agreement with recent results (e.g Pratt et al. 2009; Mantz et al. 2010). This might suggest that the observed break in the slope of the $M-L_X$ relation is a direct consequence of the physical properties of the galaxy clusters within the REFLEX II sample. A thorough analysis taking into account both the evolution of the halo mass function and the evolution of the full $M-L_X$ relation is required in order to draw more solid conclusions

about the shape of the scaling relation as demanded from the observed abundance.

Our set of mock catalogues reproduce the observed abundance of the REFLEX II sample as well as the observed two-point clustering statistics of this data-set. Therefore, they provide an excellent tool to test the statistical methods applied to the real data and to perform error analysis, especially through the covariance matrix of the cluster power spectra or the correlation function. The covariance matrix derived from this suite of catalogues properly accounts for physical effects such as the non-linear evolution of clustering, its connection to the underlying scaling relations, as well as the effect of the survey window function. This represents a major advantage of our set of mock catalogues against theoretical estimations of covariance matrices or log-normal catalogues. Our results also show that the distribution function of the values of $P(k)$ and $\xi(s)$ obtained from the individual mocks are well described by the prediction for a Gaussian distribution. This indicates that it is possible to assume a Gaussian likelihood function when comparing measurements of these statistics with the predictions from cosmological models.

In the coming years, the next generation of galaxy cluster surveys will probe much larger volumes than any present-day sample. For example, the *eROSITA* cluster survey is expected to contain approximately 10^5 objects (with $\sim 10^3$ with measured redshifts) (e.g Pillepich et al. 2011) spanning a wide range of masses over a volume of $\sim 10^2 \text{ Gpc}^3$. The construction of the mock catalogues necessary for the analysis of the large-scale clustering of this sample will demand a great effort. This task will require a suite of extremely large N-body simulations with a unique combination of volume and resolution to construct mock catalogues in the form of light-cones up to a redshift ~ 1.5 . The implementation of baryonic physics in such simulations would be even more ambitious and these mock catalogues will need to rely on more indirect methods like the one discussed here. Although the volume of the REFLEX II sample allowed us to implement a few simplifications such as the use of a single snapshot of the simulations, the scheme we have implemented to calibrate the $M-L_X$ relation can be extended to light-cones spanning wider redshift ranges, providing a simple technique to construct mock catalogues out of pure dark matter simulations even for these large samples.

ACKNOWLEDGMENTS

We thank our anonymous referee for helping suggestions and comments that greatly improved the quality of the paper. We thank Raúl Angulo and Carlton Baugh for providing us with the L-BASICC II simulations. We also thank Sarhud More for providing us with the correction for resolution effects in the FOF masses adapted to the L-BASICC II simulations. This research was in part supported by the DFG cluster of excellence “Origin and Structure of the Universe”. CAC acknowledges support from STFC. This publication contains observational data obtained at the ESO La Silla observatory.

REFERENCES

- Milton Abramowitz & Irene Stegun, *Handbook of mathematical functions*, Dover Publications, New York 1972
- Angulo R., Baugh C. M., Frenk C. S., Lacey G.C., 2008, MNRAS, 383, 755
- Balaguera-Antolínez A., Sánchez A.G., Böhringer H., Guzzo L., Collins C., Phleps S., 2011, MNRAS, 413, 386
- Behroozi S., Conroy C., Wechsler R. H., 2010, ApJ, 717, 379
- Böhringer H. et al., 2001, A&A, 369, 826
- Borgani S., 2001, ApJ, 561, 13
- Borgani S., Finoguenov A., Kay S. T., Ponman T. J., Springel V., Tozzi P. and Voit G. M., 2005, MNRAS, 361, 233
- Cabre A., Gaztañaga E., 2009, MNRAS, 396, 1119
- Cai Y.-C., Angulo R. E., Baugh C. M., Cole S., Frenk C., 2009, MNRAS, 395, 1185C
- Cohn J.D., 2006, New Astron. Rev., 11, 226
- Cole S. et al., 2005, MNRAS, 362, 505
- Coles P. and Jones B., 1991, MNRAS, 248, 1
- Collins C., et al., 2000, MNRAS, 319, 939
- Crocce M., Fosalba P., Castander F. J. and Gaztañaga E., 2010, MNRAS, 403, 1353
- Evrard A. E. et al. 2002, ApJ 573, 7
- Fabjan D., Borgani S., Rasia E., Bonafede A., Dolag K., Murante G., Tornatore L., 2011, MNRAS, 416, 801
- Feldman H., Kaiser N., Peacock J. A., 1994, ApJ, 426, 23
- Felten J. E., 1977, AJ, 82, 861
- Guzzo L. et al., 2009, A&A, 499, 357
- Jenkins A., Frenk C., White S. D. M., Colberg J.M., Evrard A.E., Couchman H.M.P., Yoshida N., 2001, MNRAS, 312, 372
- Kay S. T., da Silva A. C., Aghanim N., Blanchard A., Lidde A. R., Puget J-L., Sadat R. and Thomas P., A, 2007, MNRAS, 377, 317
- Lukić Z., Reed D., Heitmann K., 2009, ApJ, 692, 217
- Maughan, N. J., 2007, ApJ 668, 772
- Mantz A., Allen S., Ebeling H., Rapetti D., Drlica-Wagner A., 2010, MNRAS, 406, 2397
- More S., Kravtsov A., Dalal N., Gottlöber S., 2011, ApJS, 195
- McBride C., Berlind A., Scoccimarro R., Wechsler R., Busha M., Gardner J., van den Bosch F., 2009, A&A 213, 426.06
- Neal R., Technical Report CRG-TR-93-1, Probabilistic Inference Using Markov Chain Monte Carlo Methods, University of Toronto
- Norberg P., Gaztañaga E., Baugh C. M., Croton D. J., 2011, MNRAS, 418, 2435
- Percival W. J. et al., 2010, MNRAS, 401, 2148
- Percival W. J., Verde L., Peacock J. A., 2004, MNRAS, 347, 645
- Pillepich A., Porciani C., Reiprich T., 2012, MNRAS, 442, 44
- Pratt G. W., Croston H. J., Arnaud M., Böhringer H., 2009, A&A 498, 361
- Press H., Teukolski S., Vetterling W., Flannery B. 2002, *Numerical Recipes in C*, Cambridge University Press.
- Puchwein E., Sijacki D., Springel V., 2008, ApJ, 687, L53
- Reichert A., Böhringer H., Fassbender R., Mühlegger M., 2011, A&A, 53, 4
- Reiprich T., 2006, A&A, 453, L39
- Reiprich T., Böhringer H., 1999, AN, 320, 296
- Retzlaff J., Borgani S., Gottlöber S., 1998, NewA, 3, 631
- Rykoff E.S. et. al., 2008, MNRAS, 387, 28
- Sánchez A. G., Baugh C. M., Angulo R., 2008, MNRAS, 4, 1470
- Sánchez A. G., Crocce M., Cabré A., Baugh C. M., Gaztañaga E., 2009, MNRAS, 400, 1643
- Schuecker P. et al., 2001, A&A 368, 86
- Schuecker P., Böhringer H., Collins C., Guzzo L., 2003, A&A 398, 867
- Short C. J., Thomas P. A., Young O. E., Pearce F. R., Jenkins A. and Muanwong O., 2010, MNRAS, 408, 2213
- Smith R. E., Scoccimarro R., Sheth R.K., 2008, Phys. Rev D, 77, 043525
- Smith R. E., 2012, preprint (arXiv:1205.4240),
- Spergel D. N. et al., 2007 APJSS, 170
- Springel V. et al. 2005, Nature, 435, 629
- Stanek R., Evrard A. E., Böhringer H., Schuecker P., Nord B., 2006, ApJ, 209, 17
- Stanek R., Rudd D., Evrard A. E., 2009, MNRAS, 394, L11
- Stanek R., Rasia E., Evrard A. E., Pierce F., Gazzola L., 2010, ApJ, 715, 1508
- Y. Suto Y., Magira H., Yamamoto K., 2000, PASJ, 52, 249
- Teyssier R. et al. 2009, A&A, 497, 335
- Tinker J., Kratsov A. V., Abazajian K., Warren M, Yepes G., Gottlöber S., Holz D. E., 2008, ApJ, 688, 709
- Truemper J., 1993, Science 260, no. 5115, 1769
- Tsallis C., 2009, Introduction to Nonextensive Statistical Mechanics, Springer Verlag, NY
- Vikhlinin A. et al., 2009, ApJ, 692, 1033-1059
- Voit G. M., 2005, Rev. Mod. Phys. 77, 207
- Warren M., Abazajian K., Holz D., Teodoro L., 2006, ApJ, 646, 881